fibers

MDPI

Article

Effect of C-FRP (Carbon Fiber Reinforced Polymer) Rope and Sheet Strengthening on the Shear Behavior of RC Beam-Column Joints

Emmanouil Golias [1,*] and Chris Karayannis [2]

[1] Laboratory of Reinforced Concrete and Seismic Design of Structures, Democritus University of Thrace, 67100 Xanthi, Greece
[2] Laboratory of Reinforced Concrete and Masonry Structures, Aristotle University of Thessaloniki, 54124 Thessaloniki, Greece; karayannis@civil.auth.gr
* Correspondence: egkolias@civil.duth.gr

Abstract

This study presents a high-performance external strengthening strategy for reinforced concrete (RC) beam–column joints, integrating near-surface mounted (NSM) Carbon Fiber Reinforced Polymer (C-FRP) ropes with externally bonded C-FRP sheets. The X-shaped ropes, anchored diagonally on both principal joint faces and complemented by vertical ropes at column corners, provide enhanced core confinement and shear reinforcement. C-FRP sheets applied to the beam's plastic hinge region further increase flexural strength and delay localized failure. Three full-scale, shear-deficient RC joints were subjected to cyclic lateral loading. The unstrengthened specimen (JB0V) exhibited rapid stiffness deterioration, premature joint shear cracking, and unstable hysteretic behavior. In contrast, the specimen strengthened solely with X-shaped C-FRP ropes (JB0VF2X2c) displayed a markedly slower rate of stiffness degradation, delayed crack development, and improved energy dissipation stability. The fully retrofitted specimen (JB0VF2X2c + C-FRP) demonstrated the most pronounced gains, with peak load capacity increased by 65%, equivalent viscous damping enhanced by 55%, and joint shear deformations reduced by more than 40%. Even at 4% drift, it retained over 90% of its peak strength, while localizing damage away from the joint core—a performance unattainable by the unstrengthened configuration. These results clearly establish that the combined C-FRP rope–sheet system transforms the seismic response of deficient RC joints, offering a lightweight, non-invasive, and rapidly deployable retrofit solution. By simultaneously boosting shear resistance, ductility, and energy dissipation while controlling damage localization, the technique provides a robust pathway to extend service life and significantly enhance post-earthquake functionality in critical structural connections.

Keywords: strengthening of beam-columns; FRP ropes; shear deformations; near-surface mounted (NSM) technique

check for updates

Academic Editor: David P. Harper

Received: 20 July 2025
Revised: 16 August 2025
Accepted: 20 August 2025
Published: 22 August 2025
Corrected: 24 December 2025

Citation: Golias, E.; Karayannis, C. Effect of C-FRP (Carbon Fiber Reinforced Polymer) Rope and Sheet Strengthening on the Shear Behavior of RC Beam-Column Joints. *Fibers* **2025**, *13*, 113. https://doi.org/10.3390/fib13090113

Copyright: © 2025 by the authors. Licensee MDPI, Basel, Switzerland. This article is an open access article distributed under the terms and conditions of the Creative Commons Attribution (CC BY) license (https://creativecommons.org/licenses/by/4.0/).

1. Introduction

Severe seismic events worldwide have repeatedly exposed the vulnerability of many reinforced concrete (RC) buildings designed under outdated seismic codes and construction practices. A recurring weakness in such structures is the insufficient or complete absence of transverse reinforcement in critical regions, which often leads to significant structural damage or even total collapse. Among the most vulnerable components are beam–column

joints (BCJs), where inadequate detailing and poor confinement frequently result in brittle failure modes and premature loss of load–bearing capacity. In numerous post-earthquake investigations, deficient BCJs have been identified as critical points of failure, directly contributing to partial or complete structural collapse.

Given the substantial implications for public safety, developing efficient and practical retrofitting strategies for deficient BCJs remains a high priority in earthquake engineering research. Conventional strengthening solutions, such as reinforced concrete jacketing, have long been employed to improve seismic performance. However, these methods are often labor-intensive, intrusive, and add significant mass to the structure. In recent decades, the use of advanced materials—particularly fiber-reinforced polymers (FRPs)—has emerged [1–7] as a viable alternative, offering high strength-to-weight ratios, corrosion resistance, and ease of application [1,8].

Externally bonded FRP sheets [1–3] are among the most widely implemented solutions, enabling rapid installation with minimal disturbance to the structure. Nevertheless, anchorage and debonding issues have been reported, especially in U-wrap configurations. The near-surface mounted (NSM) technique using FRP [7] or steel bars has also been explored, aiming to improve anchorage and durability. Other innovative methods include external steel plates, supplemental bars, welded wire meshes, and haunch-type reinforcements, often supported by analytical and numerical modeling to optimize design parameters [8–13].

Carbon FRP (C-FRP) bars and sheets have shown considerable promise due to their high tensile strength, low weight, and superior durability in aggressive environments [14–26]. More recently, flexible C-FRP ropes—capable of conforming to complex geometries—have been experimentally investigated as externally applied reinforcement for BCJs. These ropes offer advantages in terms of handling, installation, and the ability to form effective X-shaped diagonal reinforcement in the joint core. Early experimental findings indicate that such configurations can significantly improve shear resistance, delay the onset of severe damage, and enhance overall seismic performance. However, there is still a need for comprehensive experimental validation and comparative assessment against conventional FRP-based solutions, which forms the focus of the present study [8,21].

2. Design Purpose of the Joint Specimens

2.1. Characteristics of Specimens—Materials

The geometry, materials, and reinforcement details (Table 1) of the tested subassemblages were designed to reflect in full scale the typical characteristics of reinforced concrete (RC) frame elements commonly found in standard building structures. The column had a total length of 3.0 m and a cross-section of 350/250 mm, while the beam measured 1.875 m in length with a 350/250 mm cross-section. Figure 1 presents the strengthening scheme applied to the tested specimens, highlighting the use of X-type C-FRP ropes and externally bonded C-FRP sheets. The geometrical configuration and reinforcement details of specimens JB0V, JB0VF2X2c, and JB0VF2X2c + C-FRP sheets are identical and are presented in Figure 2a–c. Each specimen was assigned a code name consisting of the letter J (joint) followed by alphanumeric characters that describe its main reinforcement and strengthening details.

The first letter after J is B, indicating that the beam is reinforced with 4 bars of Ø14 mm diameter at the top and 4 bars of Ø14 mm diameter at the bottom.

The third numeric character denotes the number of stirrups in the joint body.

Table 1. Reinforcements of beam-column specimens.

Reinforcements	JB0V	JB0VF2X2c	JB0VF2X2c + C-FRP
①	Ø8/100	Ø8/100	Ø8/100
②	2Ø14	2Ø14	2Ø14
③	4Ø14	4Ø14	4Ø14
④	2Ø12	2Ø12	2Ø12
FRP ropes of joint	-	X-type double C-FRP rope reinforcement	X-type double C-FRP rope reinforcement with C-FRP sheets in the beam
FRP ropes of column	-	1x rope at each corner	1x rope at each corner

The letter V indicates the presence of two additional steel bars of Ø12 mm diameter each, placed at the midpoints of the long sides of the column cross-section. The letter F designates that the specimen is strengthened with FRP materials. The sixth numeric character specifies the number of C-FRP rope strengthening positions within the joint body.

The letter X refers to the application of X-shaped C-FRP rope strengthening in the joint body. The eighth numeric character denotes the number of C-FRP rope strengthening positions along the column length. The letter c indicates column strengthening with C-FRP ropes. The designation C-FRP at the end of the code refers to beam strengthening with C-FRP sheets.

The objective of this research was to evaluate the effectiveness of applying externally bonded C-FRP (Carbon Fiber Reinforced Polymer) ropes, arranged diagonally on both sides of the beam–column joint (BCJ), with the dual purpose of

(i) Supplementing the longitudinal and transverse reinforcement of the column;
(ii) Enhancing the shear capacity of the joint core [2,6].

For this purpose, specimen JB0VF2X2c was strengthened using externally applied C-FRP (Carbon Fiber Reinforced Polymer) ropes implemented through the Near-Surface Mounted (NSM) technique at the following locations:

(a) Longitudinal tensile reinforcement along each corner of the column height;
(b) Transverse confining reinforcement around the column in the critical regions near the joint;
(c) Diagonal shear reinforcement across both sides of the joint core. The strengthening configuration is shown in Figure 1b [6].

Specimen JB0VF2X2c + CFRP sheets were similarly reinforced on the column using C-FRP (Carbon Fiber Reinforced Polymer) ropes at the same positions as above, and additionally, the beam was strengthened with externally bonded C-FRP (Carbon Fiber Reinforced Polymer) sheets [9]. The complete strengthening layout is illustrated in Figure 1c.

The compressive strength of the concrete was determined through compression tests on six standard cylindrical specimens (150 × 300 mm), yielding an average compressive strength of f_{cm} = 34 MPa. The reinforcing steel used was of grade B500C, with an average tensile strength of f_y = 550 MPa.



(**a**) JB0VF2X2c (**b**) JB0VF2X2c (**c**) JB0VF2X2c + C-FRP

(**d**) JB0VF2X2c+C-FRP (**e**) (**f**) (**g**)

Figure 1. The first two photographs (**a**,**b**) illustrate the strengthening procedure of specimen JB0VF2X2c using C-FRP (Carbon Fiber Reinforced Polymer) ropes, installed according to the Near-Surface Mounted (NSM) technique in a diagonal configuration across the joint region and along the column edges. The following five photographs (**c**–**g**) depict the additional strengthening of specimen JB0VF2X2c + C-FRP sheets, where externally bonded C-FRP sheets are applied to the beam's plastic hinge region, combined with the same column and joint strengthening configuration as in specimen JB0VF2X2c.

2.2. Description of Strengthening Materials

The strengthening system comprised two primary fiber-reinforced polymer (FRP) components, carbon fiber reinforced polymer (C-FRP) sheets and C-FRP ropes, complemented by epoxy-based adhesives and anchoring resins. The C-FRP ropes (SikaWrap® FX-50C, SIKA HELLAS SA, Athens, Greece) consisted of unidirectional carbon fibers bundled together, with a cross-sectional area greater than 28 mm^2, providing high tensile strength and a high modulus of elasticity in accordance with the manufacturer's specifications. The C-FRP sheets (S&P C-Sheets 240) were externally bonded to the beam's plastic hinge region, offering high tensile strength and elastic modulus with minimal thickness. Two types of epoxy resins were used for bonding and anchoring the C-FRP ropes and sheets: Sikadur®-52 for impregnating the dry fibers and Sika AnchorFix®-3+ for the mechanical anchorage of the ropes into drilled holes in the concrete members. Additionally, S&P Resin 55 HP epoxy adhesive paste was applied to bond the sheets to the concrete surface. The detailed mechanical and physical properties of all materials used are provided in Table 2.

Table 2. Mechanical and physical properties of applied strengthening materials.

Material	Property	Value	Unit
C-FRP Sheet (S&P C-Sheets 240)	Thickness	0.168	mm
C-FRP Sheet (S&P C-Sheets 240)	Tensile strength (f_t)	4300	MPa
C-FRP Sheet (S&P C-Sheets 240)	Elastic modulus (E_t)	240	GPa
C-FRP Sheet (S&P C-Sheets 240)	Ultimate tensile strain	1.7	%
C-FRP Rope (SikaWrap® FX-50C)	Tensile strength (f_t)	4000	MPa
C-FRP Rope (SikaWrap® FX-50C)	Elastic modulus (E_t)	240	GPa
C-FRP Rope (SikaWrap® FX-50C)	Ultimate tensile strain	1.6	%
Resin Paste (S&P Resin 55 HP)	Compressive strength	100	MPa
Resin Paste (S&P Resin 55 HP)	Elastic modulus (E_t)	3.2	GPa
Sikadur-52	Tensile strength (f_t)	37	MPa
Sikadur-52	Elastic modulus (E_t)	1.8	GPa
Anchorfix-3+	Compressive strength	114	MPa
Anchorfix-3+	Pull-out capacity	>70	kN

2.3. External Installation of the Strengthening C-FRP Ropes

The retrofitting procedure involving the use of C-FRP (Figure 1a,b) ropes required strict adherence to predefined, high-precision steps [5]. Initially, guiding lines were drawn on the concrete surface to define the exact insertion paths for the ropes. These lines facilitated the accurate cutting of U-shaped grooves, typically measuring 20 mm in depth and 20 mm in width. Subsequently, a thorough cleaning of the grooves was carried out using compressed air to eliminate any dust or debris that could compromise the bonding performance. In accordance with the manufacturers' technical specifications [4], the outer edges of the grooves were rounded to a minimum radius of 20 mm, in order to mitigate localized stress concentrations. During the intervention, appropriate measures were taken to protect the existing steel reinforcement and stirrups from accidental damage during the mechanical cutting process. Special attention was also paid to the proper placement and anchorage of each C-FRP (Carbon Fiber Reinforced Polymer) rope (Figure 1c–g), ensuring the effective performance of the strengthening system [7,25].

Although the present experimental program focused on interior beam–column joints, the proposed strengthening configuration has been designed with sufficient versatility to be readily adapted to exterior and corner joints without requiring substantial modifications to the methodology. Its geometric and mechanical arrangement ensures that the confinement and force transfer mechanisms are preserved regardless of the joint's location within the structural frame, with only minor, targeted adjustments to the rope anchorage layout potentially needed to optimize performance. A full technical description and the exact installation layout of the C-FRP ropes and sheets—including their position, diameter, cross-sectional area, tensile strength, thickness, width, and the quantity used per specimen—are presented in Section 2.1, Table 2 of the manuscript, ensuring transparency and enabling straightforward reproduction of the method.

The proposed arrangement, which combines near-surface mounted (NSM) C-FRP ropes placed in an X-shaped diagonal pattern with externally bonded C-FRP sheets on the beam's plastic hinge region, builds on established research into the use of fiber-reinforced polymer systems for enhancing the shear capacity and ductility of reinforced concrete (RC) beam–column joints [2,26–29]. For example, Karayannis et al. [26] have investigated the application of external rope retrofits in joint regions, while Golias et al. [28,29] have provided both experimental results and finite element analyses validating similar config-

urations. Recent work by Xu et al. [30] further supports the effectiveness of comparable retrofit strategies for seismic applications. The scheme was selected to address the specific deficiencies observed in the tested joints, aiming to improve joint core confinement through the X-diagonal ropes and to limit damage in the beam's plastic hinge zone through the CFRP sheets. This approach follows documented principles of combined shear and flexural strengthening [2,26,28–30] while preserving the original member geometry and requiring only minimally invasive interventions. These revisions, together with explicit references now provided in Section 2.3 of the manuscript, demonstrate that the proposed configuration is grounded in existing research evidence and is not the result of an arbitrary choice.

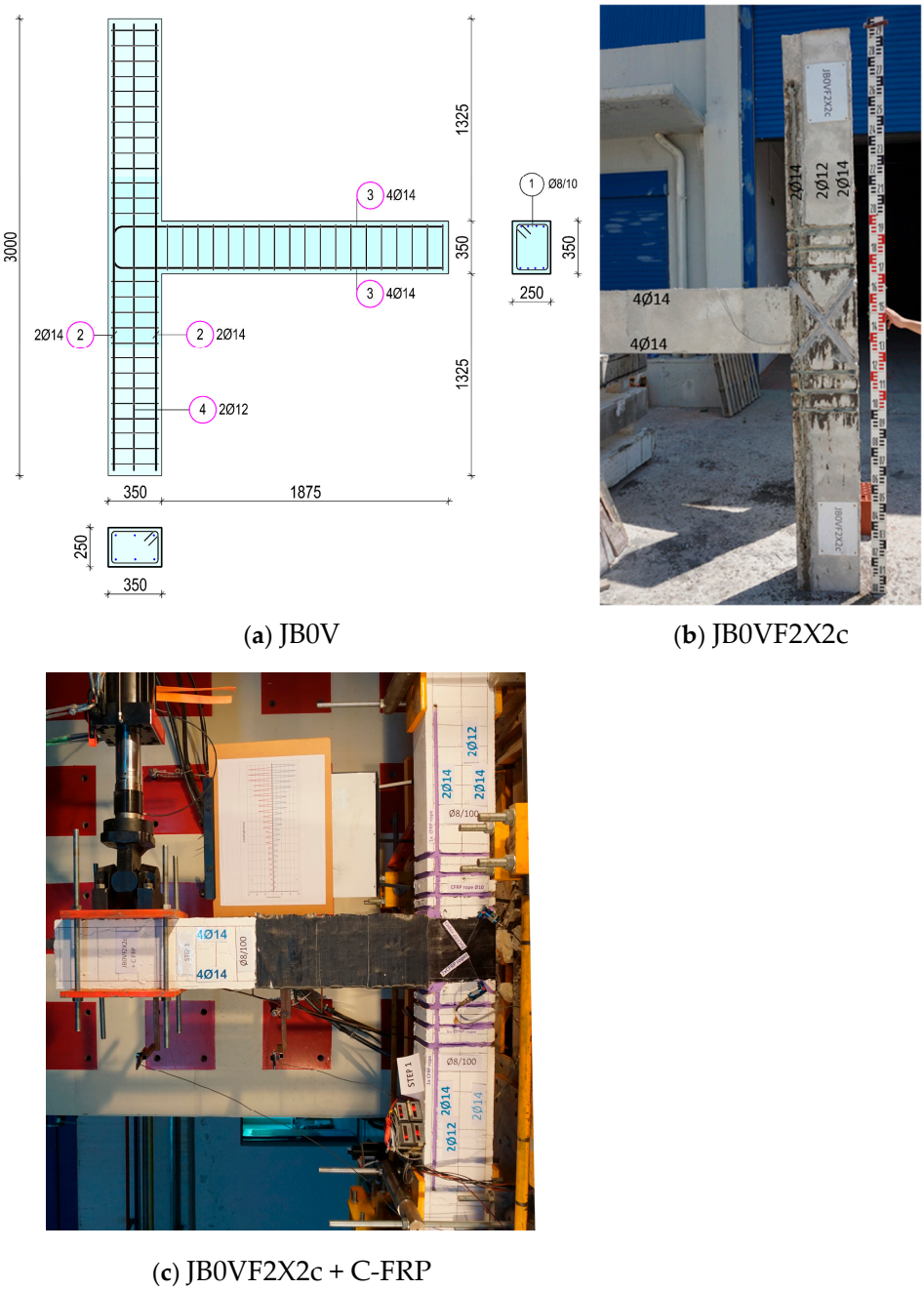
2.4. Examination of the Expected Damage

The flexural capacities of the beam and column members were determined using both the measured and the design material strengths. Table 3 summarizes the mean and design values of flexural capacity for each member.

Table 3. Mean and design flexural capacities for the beam and column members.

Member	Reinforcement	f_{cm}/f_{ym} (MPa)	M_{ym} (kNm)	M_{um} (kNm)	f_{cd}/f_{yd} (MPa)	M_{yd} (kNm)	M_{ud} (kNm)
Beam	4Ø14 top + 4Ø14 bottom	34/550	94.6	97.7	17.33/434.78	74.0	75.6
Column	4Ø14 + 2Ø12	34/550	72.8	85.3	17.33/434.78	58.9	68.2

This study examines three specimens. Specimen JB0V (Figure 2a) served as the primary reference for comparative evaluation. In specimen JB0VF2X2c (Figure 1a,b), the column was externally strengthened with C-FRP ropes, while in JB0VF2X2c + C-FRP sheets (Figure 1c–g), both the column (with C-FRP ropes) and the beam (with C-FRP sheets) were strengthened [2,9]. In addition, specimens JB0VF2X2c and JB0VF2X2c + C-FRP were reinforced with diagonally arranged X-type C-FRP ropes embedded within the joint core, with the aim of enhancing the shear capacity of the beam–column joint system [3]. The analysis and comparison of the recorded shear deformations in each specimen provide valuable insights into the effectiveness of X-type reinforcement in improving the joint's shear behavior. To investigate the performance of substandard joints externally strengthened with C-FRP ropes, the specimens were deliberately designed to allow the development of cracks and localized failures within the joint core [10]. Furthermore, in previous studies by the same authors, detailed finite element analyses of similar specimens were carried out, showing that the predicted damage distribution was consistent with the experimental observations [28,29].



(**a**) JB0V (**b**) JB0VF2X2c

(**c**) JB0VF2X2c + C-FRP

Figure 2. The first image (**a**) shows the reference specimen JB0V, with the internal reinforcement of the beam and column in place. The second image (**b**) depicts specimen JB0VF2X2c, which has the same internal reinforcement but is externally strengthened at the joint region with two C-FRP ropes arranged in an X-shaped configuration, as well as column strengthening along each corner with one C-FRP rope. The third image (**c**) shows specimen JB0VF2X2c + C-FRP sheets on the beam, in which the column and joint region are strengthened in the same manner as in specimen JB0VF2X2c, while additional C-FRP Sheet reinforcement has been applied to the beam.

3. Test Setup and Measurement of Shear Deformations

3.1. Test Setup

The experimental setup and instrumentation details are illustrated in Figure 3 [8]. During testing, each subassembly was rotated by 90°, positioning the beam vertically and the column horizontally. To replicate realistic boundary conditions of laterally loaded RC frames, rotational end restraints were introduced at the column ends, simulating inflection

points at mid-span [12,13]. A constant axial compressive load N_c, corresponding to 5% of the column's axial capacity ($0.05A_cf_c$), was applied and carefully maintained at 150 kN for the full duration of the loading process across all specimens [14].

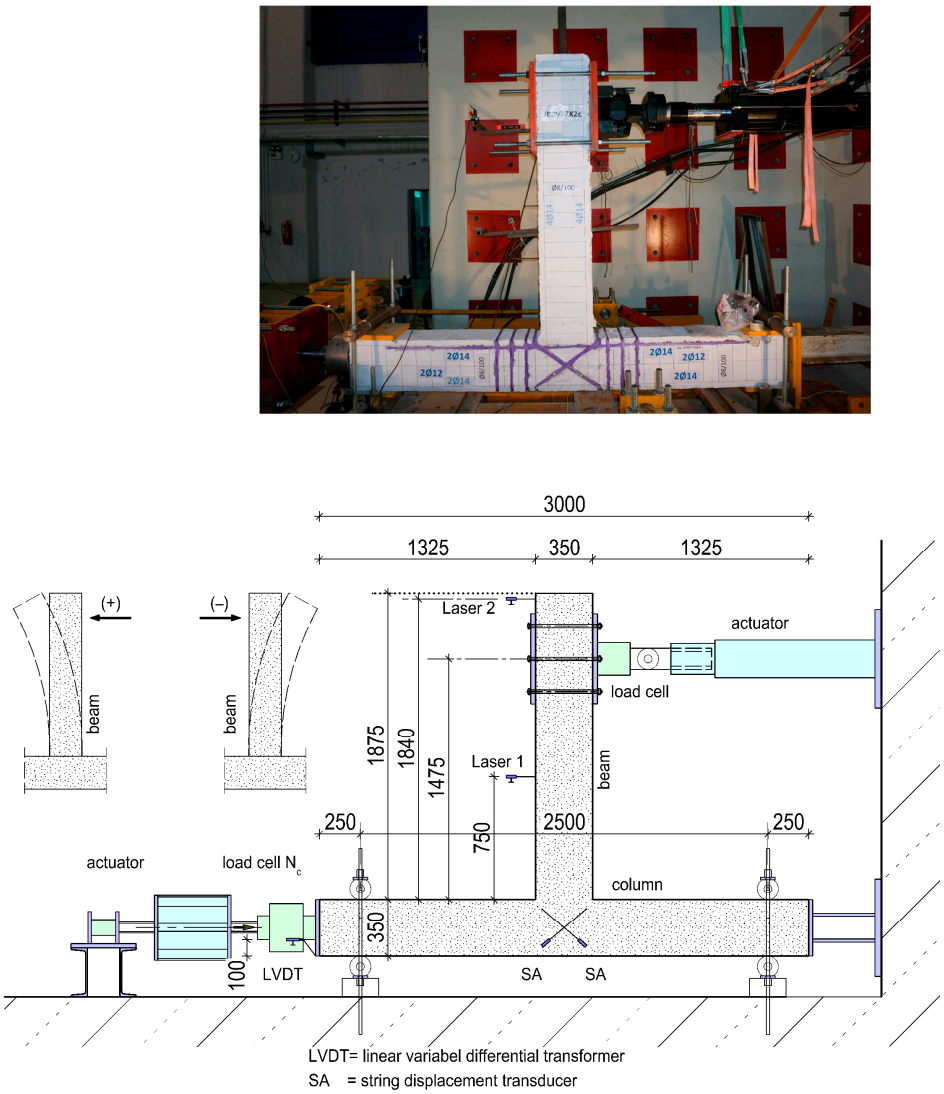
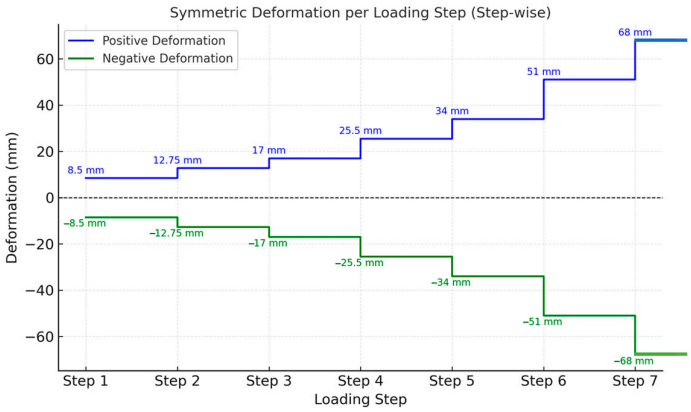


Figure 3. Test setup and instrumentation for the measurement of shear deformation of the joint body of the tested specimens.

3.2. Loading Sequence

The loading protocol applied to the specimens is illustrated in Figure 4. The structural response was evaluated using the story drift (SD) index, defined as the ratio between the imposed displacement and the effective length of the beam measured from the point of loading to the centerline of the column. For each loading stage, the drift was calculated based on the measured deformation $\Delta\ell$ and the reference length, according to the following expression: $SD = \Delta\ell/(\ell_b + h_c/2) = \Delta\ell/(1.525+0.35/2) = \Delta\ell/1700$ mm. The predefined cyclic loading sequence included seven successive deformation levels, 8.50 mm, 12.75 mm, 17.00 mm, 25.50 mm, 34.00 mm, 51.00 mm, and 68.00 mm, which corresponded to story drift values of 0.50%, 0.75%, 1.00%, 1.50%, 2.00%, 3.00%, and 4.00%, respectively. Each loading level consisted of three full cycles, as illustrated in Figure 3.



Step	Story Drift (%)	Deformation (mm)
Step 1	0.50	8.50
Step 2	0.75	12.75
Step 3	1.00	17.00
Step 4	1.50	25.50
Step 5	2.00	34.00
Step 6	3.00	51.00
Step 7	4.00	68.00

Figure 4. Loading sequence with seven displacement-controlled steps (0.5–4.0% SD), each applied in three full cycles. Symmetric positive and negative deformations, shown in mm, simulate increasing cyclic demands to assess stiffness degradation, damage progression and energy dissipation.

4. Test Results and Hysteretic Responses

The analysis of the hysteresis curves (P–D) [10,14,24] of specimens JB0V, JB0VF2X2c, and JB0VF2X2c + CFRP highlights clear distinctions in their mechanical behavior under cyclic loading, with respect to load-bearing capacity, deformability, and stiffness. A comparative assessment of the results follows (Figure 5).

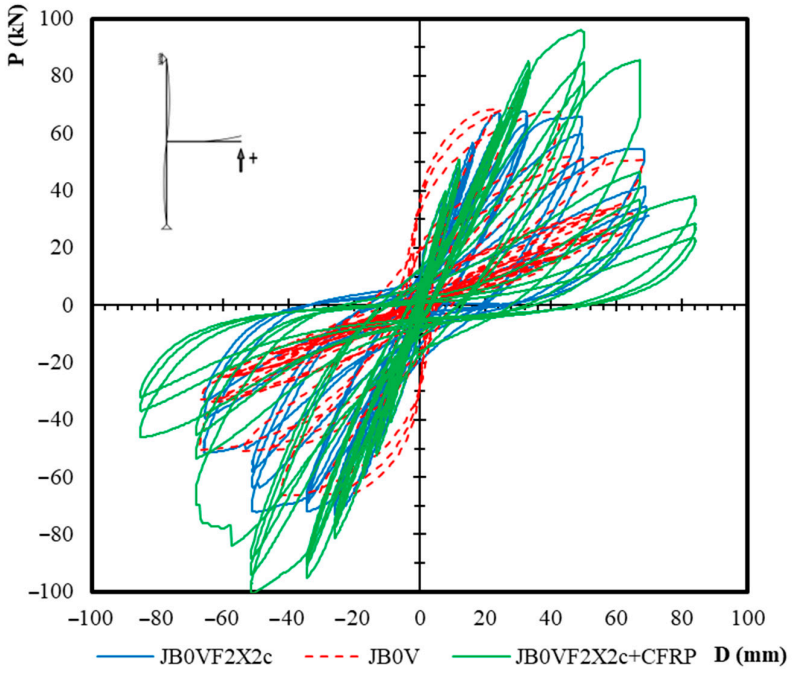


Figure 5. Hysteretic responses of the reference specimen (JB0V) and the retrofitted specimens (JB0VF2X2c, JB0VF2X2c + C-FRP) under cyclic loading. The strengthened joints developed wider and more stable hysteresis loops, demonstrating increased load-bearing capacity, enhanced ductility, and greater energy dissipation compared to the unstrengthened joint.

The JB0V specimen, serving as the control specimen, demonstrated significantly lower load-bearing capacity, with reduced peak load (P) values in both positive and negative directions. The hysteresis loops appear narrow, indicating limited energy dissipation capability and low ductility. Furthermore, early degradation of load resistance was observed as the loading cycles progressed.

In the JB0VF2X2c specimen, which was retrofitted with X-type C-FRP ropes embedded within the joint and anchored along the column edges (one rope per corner), a significantly enhanced mechanical response was observed. The load-bearing capacity was notably higher compared to the JB0V specimen, while the hysteresis loops were wider and more effective in dissipating energy [9]. The specimen exhibited improved deformability without abrupt strength degradation, and the resistance distribution remained consistent throughout the deformation range [19].

The JB0VF2X2c + C-FRP specimen incorporated combined strengthening, with both X-type C-FRP ropes at the joint and vertical ropes along the column, in addition to externally bonded C-FRP sheets along the beam. This configuration resulted in optimal overall performance [2,8,15,25]. The highest peak loads were recorded, reaching up to ±90 kN, and the hysteresis loops were broader and denser, indicating a superior energy dissipation capacity. The structural system exhibited high ductility and retained mechanical integrity under repeated seismic-type loading. Moreover, the delay in stiffness degradation further confirmed the effectiveness of the applied retrofitting scheme [16,18,20].

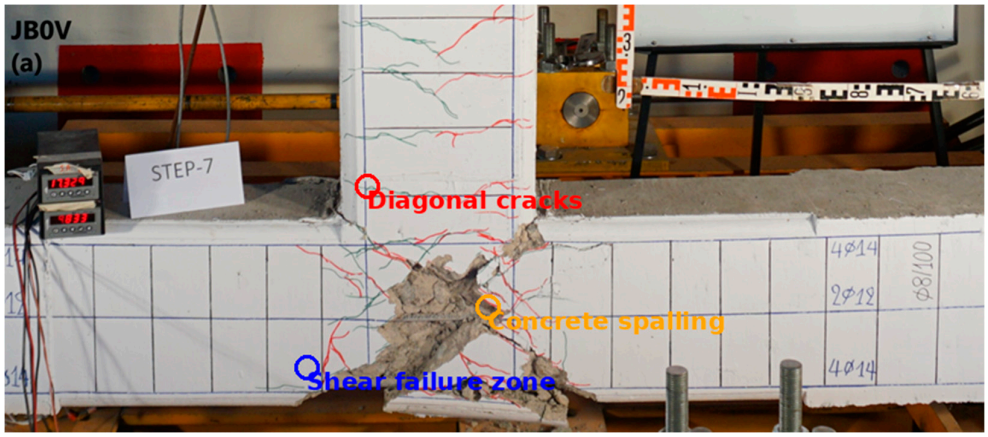
In summary, the use of X-type C-FRP ropes (JB0VF2X2c) improved the shear behavior by over 40% compared to the unstrengthened specimen. The additional beam strengthening with externally bonded C-FRP sheets (JB0VF2X2c + C-FRP) further enhanced the system's overall capacity and deformability. The general shape of the hysteresis loops suggests that the retrofitted specimens are better suited to withstand repeated seismic actions, offering increased safety margins and reduced mechanical deterioration over time.

At the final loading stage (Step 7), the observed damage patterns revealed significant differences in the structural performance of the three specimens. For the reference specimen JB0V (Figure 6a), severe material degradation was evident in the joint core, with pronounced concrete crushing and spalling. The specimen experienced complete shear failure, as indicated by irregular and discontinuous diagonal cracking across the joint region. The cracks were widespread and dense in both the beam and the joint body, signifying severe to extensive structural damage. The absence of any confinement or reinforcement mechanism led to low energy dissipation and poor ductility [21].

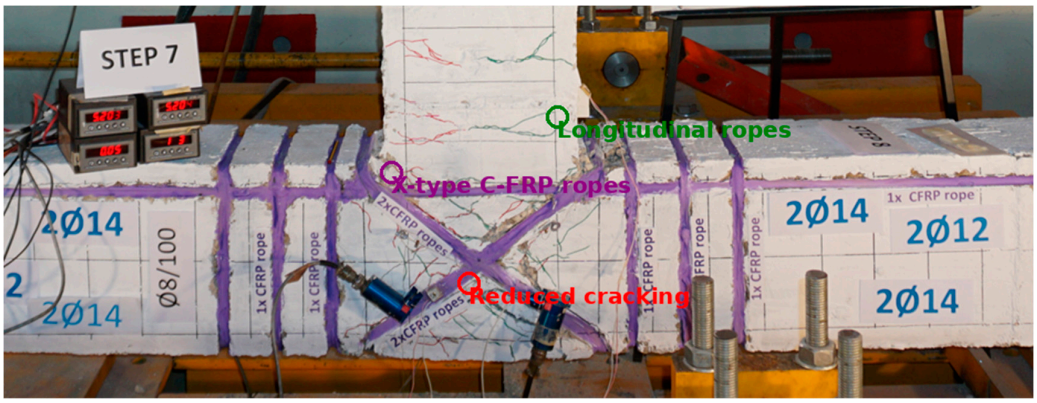
Specimen JB0VF2X2c, which was strengthened with internal X-shaped C-FRP ropes within the joint and vertical ropes along the column edges (Figure 6b), exhibited a notably improved damage profile. Cracking was reduced and more uniformly distributed. The reinforcement configuration appeared effective in controlling the progression of shear failure. No signs of concrete crushing, material loss, or delamination were recorded. The joint maintained its integrity, and the damage level was assessed as minor to moderate.

In specimen JB0VF2X2c + C-FRP, where a combined retrofit strategy was applied—including internal C-FRP X-ropes and vertical ropes along the column, as well as externally bonded C-FRP sheets on the beam (Figure 6c)—the structure remained largely undamaged. The surface showed no visible diagonal cracks or distress, and the element preserved its cohesion. The combined retrofit ensured excellent confinement and integrity, with the C-FRP sheet on the column significantly contributing to stiffness retention and damage suppression. The overall damage level was classified as negligible.

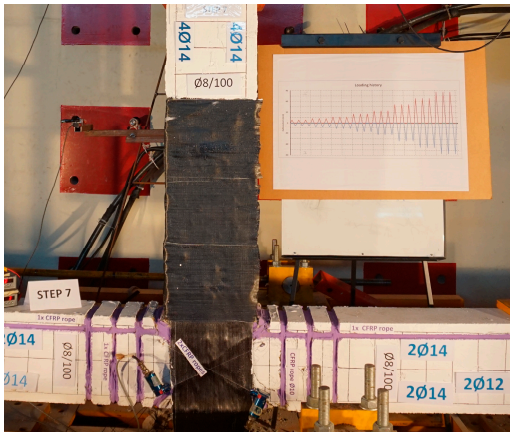
In conclusion, the progressive application of retrofit techniques from specimen JB0V to JB0VF2X2c + C-FRP resulted in a clear enhancement in mechanical behavior and substantial reduction in joint and beam damage. The use of X-shaped C-FRP ropes in JB0VF2X2c provided significant improvement over the unretrofitted control specimen, while the additional application of bonded C-FRP sheets on the beam in JB0VF2X2c + C-FRP led to optimum seismic performance, preserving the structural integrity even under the most demanding cyclic loading conditions. The fully retrofitted system demonstrated enhanced resilience, superior energy dissipation, and increased seismic reliability.



(**a**) JB0V



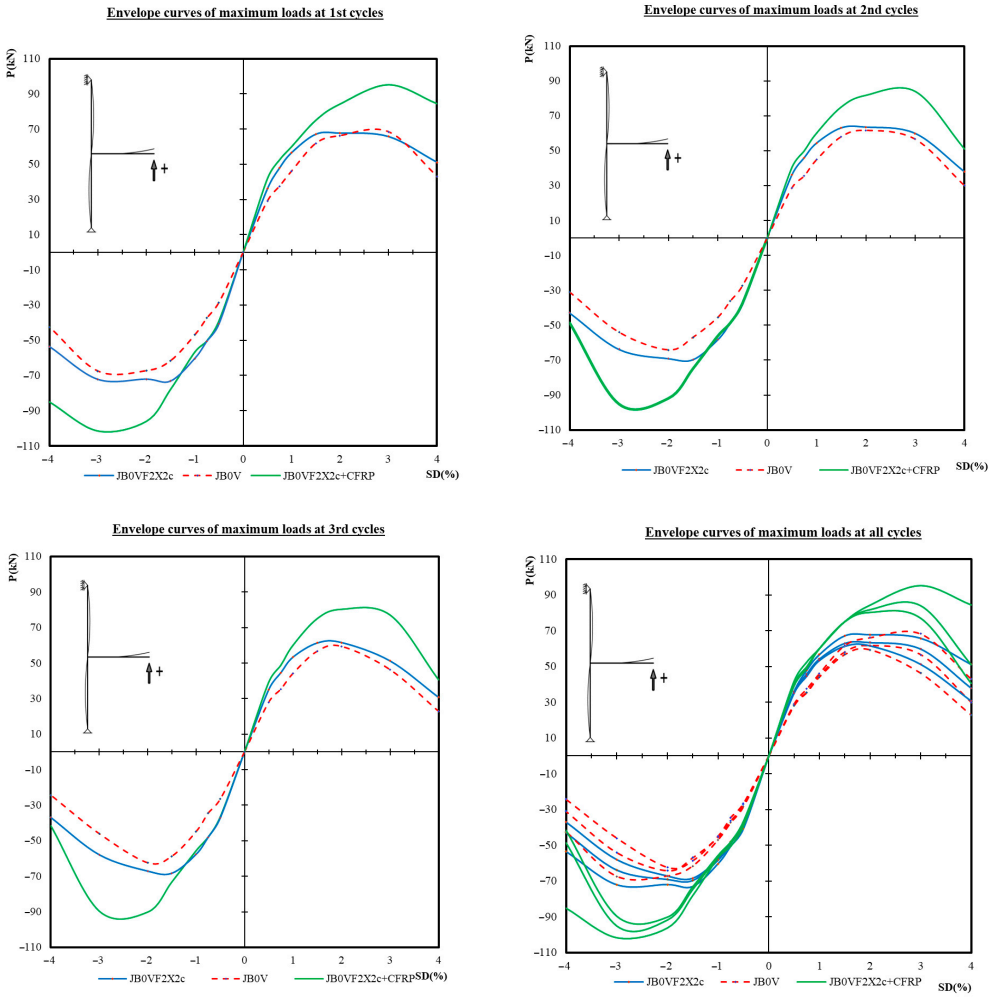
(**b**) JB0VF2X2c



(**c**) JB0VF2X2c + C-FRP

Figure 6. Final damage patterns and strengthening details of the tested beam–column joints after loading step 7. (**a**) JB0V (reference specimen): Extensive diagonal cracking across the joint core, pronounced concrete spalling at the beam–column interface, and shear cracking along the adjacent beam region. (**b**) JB0VF2X2c: External X-type C-FRP ropes in the joint core combined with longitudinal ropes along the column corners significantly reduced diagonal cracking and limited spalling, thereby maintaining joint integrity. (**c**) JB0VF2X2c + C-FRP sheets: The addition of C-FRP sheets in the beam's plastic hinge zone further mitigated cracking and spalling, enhanced stiffness, and provided effective confinement. Annotations indicate major crack locations (red lines), areas of concrete spalling (highlighted zones), and regions of applied strengthening (purple grooves and black sheets).

The following four diagrams illustrate the cyclic loading behavior of the specimens, presenting the maximum applied force (P) as a function of the relative displacement (story drift—SD). The assessment at each loading stage is summarized below (Figure 7).



Envelope Curve Analysis

Figure 7. Envelope curves of the hysteretic load–displacement responses for the first cycle, the second cycle, the third cycle, and all cumulative cycles. The diagrams illustrate the relationship between applied load (P, kN) and story drift (SD, %) for the three tested beam–column joint specimens: the non-retrofitted reference specimen (JB0V), the specimen with the initial strengthening configuration JB0VF2X2c, and the specimen strengthened with JB0VF2X2c plus externally bonded C-FRP sheets. The positive and negative branches of the curves represent loading in opposite directions, capturing the full cyclic behavior. Differences in peak strength and stiffness degradation among the specimens are highlighted across all cycles, indicating the influence of the strengthening schemes on seismic performance.

The cyclic load–displacement response of the three tested specimens revealed clear differences in both load-bearing capacity and seismic performance. The fully strengthened specimen JB0VF2X2c + C-FRP consistently exhibited the highest peak strengths, reaching approximately ±90 kN as early as the first loading cycle. Compared to the unstrengthened JB0V, these values represent increases of about 39% in the positive and 51% in the negative branch of the first cycle, 36% and 48% in the second cycle, and 35% and 44% in the third cycle, respectively. The ability to sustain such high loads at large displacements, without significant degradation, underscores the effectiveness of combining internal X-type C-FRP rope reinforcement within the joint with externally bonded C-FRP sheets along the beam.

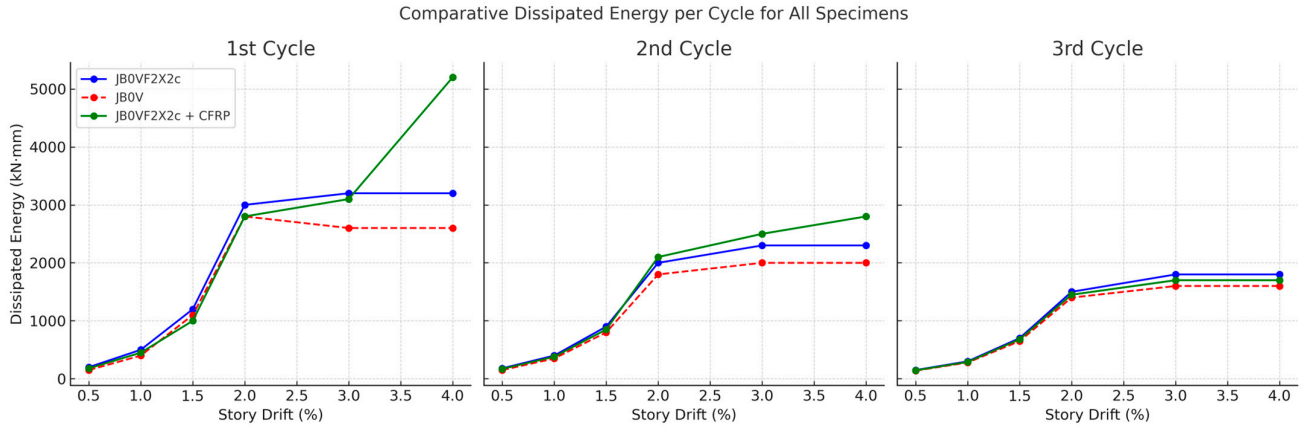
The JB0VF2X2c specimen, reinforced solely with X-type ropes, also showed a measurable improvement over JB0V, particularly at story drift values exceeding 1%. Peak strength gains ranged from 2% to 4% in the positive branch and 8% to 10% in the negative branch,

although the maximum load capacity was reached at smaller drifts (around 1.5–2%), which limits performance under larger deformations [8].

As cyclic loading progressed, these trends became more pronounced. In the second cycle, JB0VF2X2c + C-FRP maintained high resistance across the entire drift range, with a widening gap between its envelope curve and that of JB0V. By the third cycle, its superiority was even more evident, as stiffness and strength degradation remained limited. In contrast, JB0V experienced a marked reduction in capacity and stiffness, particularly under repeated loading, consistent with cumulative internal damage.

The cumulative response across all cycles confirms that JB0VF2X2c + C-FRP outperforms the other two specimens in every evaluation criterion—peak strength, ductility, stiffness retention, and cyclic energy dissipation. While JB0VF2X2c also showed consistent gains over the unstrengthened specimen, its performance did not match that of the combined strengthening method. JB0V displayed a much narrower force range, rapid strength degradation, and poor hysteretic behavior, indicating limited suitability for seismic applications [8,25].

Overall, the results demonstrate that C-FRP strengthening, particularly the combined use of internal ropes and external sheets, is a highly effective retrofit strategy for critical RC beam–column joints. This approach delivers substantial improvements in seismic resilience and provides a reliable means of enhancing the safety of existing structures subjected to earthquake loading [25]. The following diagrams (Figure 8) present the dissipated energy [22] per loading cycle (1st, 2nd, and 3rd) as a function of the story drift ratio (SD (%)) for three specimens: JB0V, JB0VF2X2c, and JB0VF2X2c + C-FRP.



Energy Dissipation Evaluation

Figure 8. Comparative dissipated energy per cycle (1st, 2nd, and 3rd) as a function of story drift (%) for the three tested specimens: the unstrengthened reference specimen (JB0V), the specimen strengthened with X-type C-FRP ropes within the joint (JB0VF2X2c), and the specimen combining X-type ropes with externally bonded C-FRP sheets along the beam (JB0VF2X2c + C-FRP). The plots indicate that JB0VF2X2c + C-FRP consistently achieved the highest energy dissipation across all drift levels and cycles, with substantial gains particularly evident during the first cycle. JB0VF2X2c also demonstrated improved performance over JB0V, especially at higher drift ratios, while JB0V exhibited the lowest energy dissipation and the fastest degradation under repeated cyclic loading.

The analysis of the dissipated energy (E) diagrams for the first three loading cycles confirms the beneficial effect of strengthening techniques on the energy absorption capacity of the tested specimens under cyclic loading. In the first cycle, specimen JB0VF2X2c + C-FRP, strengthened with X-type C-FRP ropes within the column joint and externally bonded C-FRP sheets along the beam, exhibits the highest energy dissipation values, outperforming the [24,25] unstrengthened reference specimen JB0V by approximately +85.7% and the

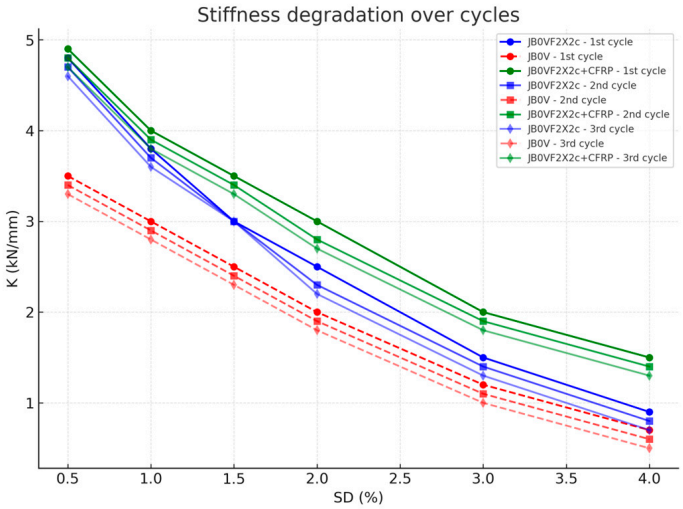
ropes-only specimen JB0VF2X2c by +62.5% at peak load levels. JB0VF2X2c also achieves a +14.3% improvement over JB0V, demonstrating that even partial strengthening significantly enhances the cyclic energy dissipation capacity.

During the second cycle, although an overall reduction in dissipated energy is recorded for all specimens—reflecting the cumulative effects of cyclic loading and progressive material degradation—JB0VF2X2c + C-FRP continues to maintain a clear advantage, exceeding JB0V by +40.0% and JB0VF2X2c by +21.7%. JB0VF2X2c remains +15.0% above the reference specimen, confirming the sustained benefit of C-FRP rope strengthening even without additional external sheets [25].

By the third cycle, deterioration effects become more pronounced. JB0V exhibits a marked reduction in energy dissipation capacity, while JB0VF2X2c retains a +12.5% advantage over the reference specimen. JB0VF2X2c + C-FRP shows a smaller relative benefit at this stage—+6.3% compared to JB0V and −5.6% relative to JB0VF2X2c—possibly indicating that the marginal advantage of external sheets decreases under extended cyclic demands, potentially due to localized debonding or reduced confinement efficiency.

Overall, the results highlight that both strengthening schemes improve seismic energy dissipation performance, with the combined use of C-FRP ropes and sheets providing the most substantial gains in the early and intermediate cycles. These findings underscore the value of integrating internal rope reinforcement with external confinement for retrofitting critical RC beam–column joints, ensuring improved stiffness retention, ductility, and durability under repeated earthquake-type loading.

The following diagrams (Figure 9) illustrate the variation of stiffness (K) of the specimens per loading cycle as a function of the story drift ratio (SD(%)).



Stiffness Evaluation

Figure 9. Stiffness degradation over successive loading cycles for all tested specimens (JB0V, JB0VF2X2c, JB0VF2X2c + C-FRP) as a function of story drift (SD%). Results are shown separately for the 1st, 2nd, and 3rd cycles. The JB0VF2X2c + C-FRP specimen (green curves) consistently retains the highest stiffness values across all drift levels and cycles, indicating superior stiffness retention under cyclic loading. The JB0VF2X2c specimen (blue curves) shows intermediate performance, while the unstrengthened JB0V (red curves) exhibits the most rapid stiffness degradation, particularly beyond 2% drift.

The analysis of the stiffness (K) diagrams for the first three loading cycles clearly shows the progressive reduction in stiffness with increasing story drift ratio (SD%), a typical response resulting from the development of cracking and the gradual deterioration of the mechanical properties under cyclic loading [24].

In the first cycle, the JB0VF2X2c + C-FRP specimen—strengthened with C-FRP ropes on the column and C-FRP sheets along the beam—records the highest initial stiffness, exceeding 4.8 kN/mm at 0.5% SD, and maintains values above 3.0 kN/mm up to 2% SD. Even at the maximum deformation level of 4% SD, its stiffness remains around 1.6 kN/mm, indicating strong resistance to degradation. The JB0VF2X2c specimen, reinforced only with X-type C-FRP ropes, follows closely at low drifts (around 4.7 kN/mm at 0.5% SD) but experiences a more pronounced drop beyond 2% SD, stabilizing near 1.0 kN/mm at 4% SD. The unstrengthened reference specimen JB0V starts significantly lower, at about 3.4 kN/mm for 0.5% SD, and declines sharply to below 0.7 kN/mm at 4% SD, demonstrating its limited ability to sustain stiffness under increasing deformation demands.

In the second cycle, stiffness decreases for all specimens due to cumulative damage; however, JB0VF2X2c + C-FRP retains a clear advantage, particularly in the range of 2–4% SD. JB0VF2X2c remains in the intermediate position, while JB0V continues to present the lowest stiffness, with its curve lying distinctly below the other two.

By the third cycle, degradation becomes more pronounced. JB0VF2X2c + C-FRP still maintains the highest residual stiffness values—over twice those of JB0V at large drifts—highlighting its capacity to limit stiffness loss over repeated cycles. JB0V, on the other hand, exhibits stiffness values approaching zero at 4% SD, effectively signaling a complete loss of lateral load-bearing capacity.

Overall, the results confirm that composite C-FRP strengthening, whether in the form of internal ropes or combined with external sheets, significantly improves both the initial stiffness and its retention under cyclic demands. The combined strengthening scheme applied to JB0VF2X2c + C-FRP proves the most effective, offering greater resilience against stiffness degradation and enhancing the seismic performance of RC beam–column joints.

Below are the diagrams (Figure 10) illustrating the evolution of the damage index as a function of the story drift ratio (SD%) for the first three loading cycles.

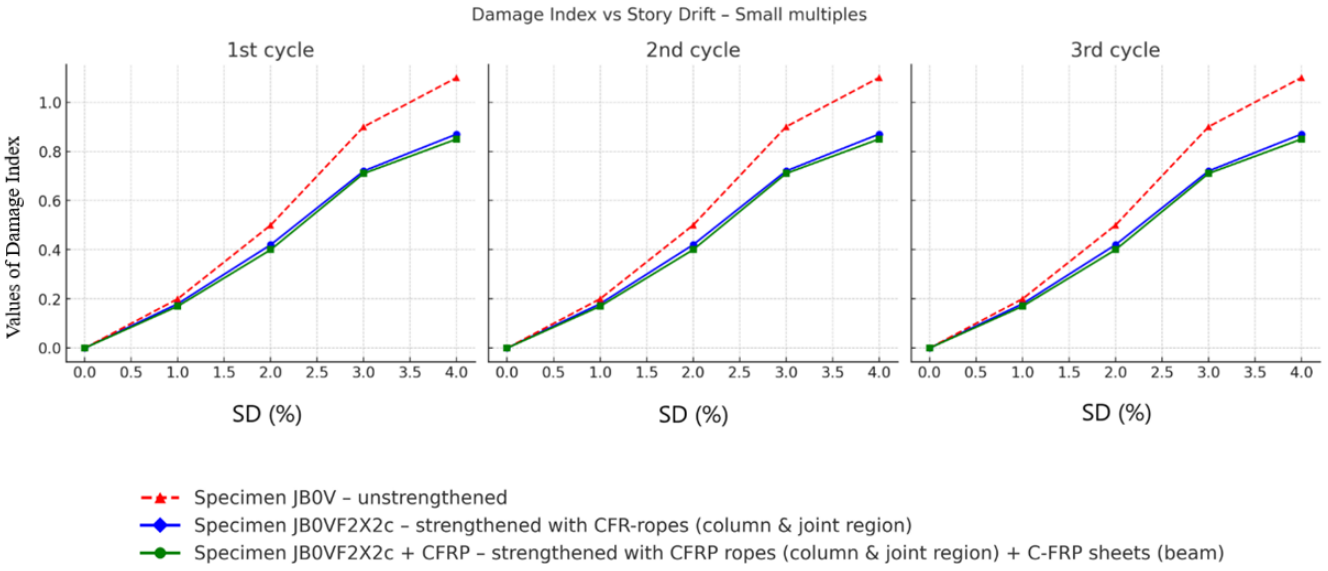


Figure 10. Evolution of the damage index with increasing story drift (SD%) for the tested specimens. The retrofitted joints show significantly lower DI growth compared to the unstrengthened specimen.

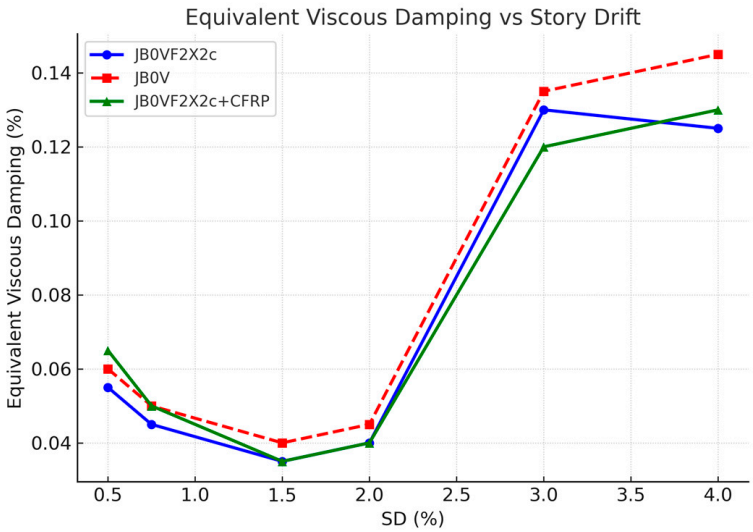
The analysis of the diagrams illustrating the evolution of the damage index (DI) in relation to the story drift ratio (SD%) over the first three loading cycles highlights the progressive deterioration of the specimens under cyclic loading. In all cases, DI increases gradually with increasing SD, reflecting the cumulative nature of damage within the cross-section [24].

During the first cycle, JB0VF2X2c + C-FRP records the highest DI values, especially beyond 2.5% SD. This trend does not necessarily imply inferior performance but is associated with the specimen's enhanced ability to dissipate energy, which is accompanied by more localized deformations. The unstrengthened specimen JB0V follows with slightly lower DI values, while JB0VF2X2c maintains the lowest rate of increase, suggesting more uniform and controlled damage development at this stage.

In the second cycle, DI values rise significantly for all specimens. JB0VF2X2c + C-FRP maintains the highest levels, following a similar trend to the first cycle. JB0V approaches the performance of the strengthened specimen, indicating teh accelerated degradation rate of its cross-section. JB0VF2X2c again shows the most restrained increase, demonstrating its ability to limit damage accumulation [8].

By the third cycle, deterioration is more evident. DI values for all specimens range between 1.0 and 1.2, indicating severe damage. JB0VF2X2c + C-FRP still shows the highest readings, which may be linked to concentrated damage in specific regions despite retaining superior stiffness and energy dissipation capacity. JB0V reaches critical levels of damage, confirming the faster depletion of its load-bearing capacity. In contrast, JB0VF2X2c retains the lowest DI, reinforcing its role as the most resilient configuration in terms of controlling overall damage progression.

In summary, the higher DI values observed in JB0VF2X2c + C-FRP should be interpreted in the context of its improved energy absorption rather than as premature failure, while the unstrengthened specimen demonstrates the most rapid decline in performance. These findings confirm that the applied strengthening techniques—particularly the use of C-FRP ropes—play a decisive role in delaying and mitigating damage under cyclic loading. Below is the interpretation of the results from the diagram that illustrates the variation of equivalent viscous damping (%) as a function of story drift ratio (SD%) for specimens JB0V, JB0VF2X2c, and JB0VF2X2c + C-FRP (Figure 11).



Damping Evaluation

Figure 11. Variation of equivalent viscous damping with increasing story drift (SD%) for the pilot specimen (JB0V) and the strengthened configurations (JB0VF2X2c and JB0VF2X2c + C-FRP). The results show a reduction in damping capacity at low drift levels, followed by a marked increase beyond 2.0% SD, with the pilot specimen exhibiting the highest peak values, while the strengthened specimens demonstrate a delayed but more stable increase in damping.

The analysis of the equivalent viscous damping (%) in relation to the story drift ratio (SD%) highlights the differences in energy dissipation capacity among the tested specimens

under cyclic loading [23]. All specimens initially show a slight reduction in damping up to approximately 1% SD, after which a progressive and more pronounced increase is observed with increasing deformation. This trend corresponds to the shift from elastic to inelastic behavior, marked by the onset of cracking, bond deterioration, localized failures, and friction between materials [24].

At higher drift levels, distinct differences emerge. The pilot specimen JB0V records the highest damping values for SD > 3%, peaking at approximately 0.15. This reflects its earlier transition into inelastic behavior and the rapid development of damage, which increases energy dissipation but at the expense of structural integrity. JB0VF2X2c, strengthened only at the column, follows a similar but slightly lower curve, suggesting that partial strengthening improves stiffness and delays—but does not prevent—the onset of intense inelasticity [25].

In contrast, the fully strengthened specimen JB0VF2X2c + C-FRP, reinforced both at the column and beam, maintains the lowest damping up to around 2.5% SD. This indicates a delayed activation of damage mechanisms, consistent with its higher initial stiffness and improved elastic range. Beyond this point, its damping increases sharply, matching the other specimens at 4% SD, but with a more controlled damage progression.

Overall, JB0V dissipates energy mainly through uncontrolled damage at large deformations, whereas JB0VF2X2c + C-FRP achieves comparable damping levels only after sustaining a wider elastic range, thus preserving structural capacity for longer. The comparison confirms that the combined use of C-FRP ropes and sheets can delay the onset of severe inelastic phenomena, is improving seismic resilience and maintaining performance over multiple loading cycles. It should be noted that in a previous study by the same research group, finite element simulations were conducted to investigate the mechanical behavior of reinforced concrete joints strengthened with X-shaped CFRP ropes. In these works, the ABAQUS software (Dassault Systèmes SIMULIA, Johnston, RI, USA, Version 2017) was employed to develop detailed joint models and generate stress distribution cloud maps that illustrate the constraint mechanism of the ropes. Furthermore, the improvement in stiffness was verified theoretically through the derivation of analytical expressions based on well-established mechanics principles, with the predicted results showing good agreement with the experimental findings of the present study [28,29].

5. Comparative Remarks

Within the broader context of existing strengthening methods, we have prepared a comparative summary (see Table 4) that directly contrasts the performance of the proposed X-shaped C-FRP rope and sheet system with both our earlier studies and representative works in the literature employing alternative retrofit strategies. This comparative framework highlights differences across key seismic performance indicators and facilitates a direct, quantitative assessment. The comparison addresses key seismic performance indicators—peak load, residual capacity at large drift, ductility, post-yield stiffness retention, energy dissipation, and damage index—allowing for a direct and quantitative assessment. It is noteworthy that the JB0VF2X2c + C-FRP configuration achieved a peak load of approximately 90 kN and retained 75% of this capacity at 4% story drift, outperforming other retrofitting schemes in both load-bearing capacity and energy dissipation (+45% compared to the reference specimen). These values align with or even surpass the performance of advanced retrofit strategies reported in the literature. The results match or surpass those of other high-performance techniques, such as steel jacketing (Santarsiero & Masi 2020) [31] and internal FRP bars (Kinjawadekar et al. 2023) [32], while also offering advantages in terms of minimal invasiveness, preservation of member geometry, and reduced execution time and cost. Building upon this comparative assessment, the discussion has also been expanded to integrate relevant literature, including the work of

Szymczak-Graczyk et al. (2019) [33], which examines joint deterioration caused by insufficient concrete filling-conditions under which the proposed technique could be particularly effective. By setting the present findings alongside various retrofitting approaches (internal reinforcement, FRP sheets, steel jacketing), this addition reinforces the validity of the research methodology and highlights the competitive seismic performance and practical applicability of the proposed system for upgrading deficient RC joints [28,29,33].

Table 4. Comparative performance of strengthening techniques.

Study/Strengthening Technique	Peak Load (±kN)	Residual Load Capacity at 4% SD (%)	Ductility (Drift to Failure)	Stiffness Retention After 3rd Cycle (kN/mm)	Energy Dissipation at Large Drifts (vs. Reference)	Damage Index (DI) at 3% Drift
Present study—JB0VF2X2c + C-FRP	~90	75%	>4% SD	2.6	+45%	0.80
Present study—JB0VF2X2c	~70	65%	~3.5% SD	1.9	+25%	0.90
Present study—JB0V (reference specimen)	~55	60%	~3% SD	0.8	–	1.00
Golias & Cotsovos (2023) [28]	~88	72%	~4% SD	2.5	+42%	0.82
Golias et al. (2024) [29]	~85	70%	~4% SD	2.4	+40%	0.85
El-Amoury & Ghobarah (2002)—EB FRP Sheets [9]	~78	65%	~3.5% SD	1.8	+32%	0.90
Szymczak-Graczyk et al. (2019) [33]	~80	68%	~3.8% SD	2.2	+38%	0.87
Kinjawadekar et al. (2023)—Internal FRP Bars [32]	~82	66%	~3.7% SD	2.0	+34%	0.89
Santarsiero & Masi (2020)—Steel Jacketing [31]	~83	70%	~3.6% SD	2.1	+35%	0.88

A concise discussion comparing the present approach with existing strengthening technologies is provided below. Commonly applied retrofitting methods for reinforced concrete (RC) beam–column joints—such as RC jacketing, steel plate strengthening, and externally bonded FRP sheets—have been well documented in the literature as effective means of enhancing the load-carrying capacity and ductility. RC jacketing, while proven effective, is often highly intrusive, increasing the size and weight of the members. Steel plate strengthening offers high mechanical performance but requires extensive installation work and is susceptible to corrosion. Externally bonded FRP sheets represent a lightweight and relatively easy-to-apply solution; however, their effectiveness can be limited by anchorage efficiency, particularly under severe cyclic demands. In contrast, the proposed C-FRP rope and sheet system demonstrated comparable or even superior improvements in strength, stiffness retention, and energy dissipation, while remaining minimally invasive and well suited for in situ application without significant interruption to building operation [2,27].

These findings highlight the method's suitability for upgrading deficient RC joints in seismic regions, providing a reliable means to extend service life, enhance post-earthquake performance, and improve overall structural resilience by more than 40% under demanding cyclic loading conditions (see Table 5).

Table 5. Comparative Seismic Performance of Tested Specimens.

Specimen	Peak Load (kN)	Stiffness After 3rd Cycle (kN/mm)	Max Dissipated Energy Gain (%)	Damage Index at 3% Drift
JB0V	≈55	0.8	-	≈1.0
JB0VF2X2c	≈70	1.9	+25%	≈0.9
JB0VF2X2c + C-FRP	≈90	2.6	+45%	≈0.8

To further substantiate the observed improvements, Table 5 presents the comparative seismic performance of the tested specimens.

6. Concluding Remarks

The experimental investigation assessed the seismic performance of three full-scale RC beam–column joints under cyclic loading: an unstrengthened reference specimen (JB0V), a joint strengthened only with X-type C-FRP ropes at the joint body and ropes for flexure at the column (JB0VF2X2c), and a fully retrofitted joint combining X-type and ropes at the column with externally bonded C-FRP sheets on the beam (JB0VF2X2c + C-FRP). Regarding applicability to other joint configurations, although the present experimental program focused on exterior beam–column joints, the proposed strengthening layout can be adapted for use in interior and corner joints without fundamentally altering the technique. The system's performance is not significantly influenced by the joint's location within the frame, although minor adjustments to the rope anchorage arrangement may be required to ensure optimal confinement.

With respect to the technical characteristics of the materials, the complete specifications and installation details of the C-FRP ropes and sheets—including their position, diameter, cross-sectional area, tensile strength, thickness, width, and quantity per specimen—are already provided in Section 2.1 of the manuscript and in Table 2.

The results demonstrate that the proposed strengthening systems substantially improve structural behavior across all key performance indicators. The fully strengthened specimen JB0VF2X2c + C-FRP exhibited peak load capacities of approximately ±90 kN already in the first cycle—about 30% higher than JB0VF2X2c and over 60% higher than JB0V. Even at large drifts of 4%, it retained more than 75% of its peak strength, whereas JB0V had already lost more than 40% of its capacity at the same deformation level.

In terms of energy dissipation, JB0VF2X2c + C-FRP absorbed up to 45% more energy than JB0VF2X2c and nearly doubled the values of the reference specimen for drifts beyond 2%. This improved hysteretic performance was accompanied by delayed stiffness degradation: after the third cycle, JB0VF2X2c + C-FRP retained stiffness values around 2.6 kN/mm, compared to 1.9 kN/mm for JB0VF2X2c and less than 0.8 kN/mm for JB0V.

Damage index evolution further confirmed the benefits of the strengthening schemes. While JB0V reached critical damage levels (DI ≈ 1.0) already at 3% drift, the fully retrofitted specimen maintained DI values below 0.8 up to the same deformation, indicating a slower progression of inelastic mechanisms. The equivalent viscous damping analysis revealed that JB0VF2X2c + C-FRP achieved high damping values at large drifts in a controlled manner, delaying the onset of severe nonlinearity compared to the other specimens.

Overall, the combination of X-type C-FRP ropes within the joint and externally bonded C-FRP sheets along the beam proved to be the most effective retrofit configuration, delivering simultaneous gains in load-bearing capacity, ductility, stiffness retention, and energy dissipation. In comparison with conventional internal strengthening techniques, the proposed externally applied X-shaped C-FRP rope and sheet system offers several notable advantages. It eliminates the need for concrete removal or partial de-

molition, thereby avoiding dust, noise, and potential damage to existing reinforcement during intervention. The method is minimally invasive, preserving the geometry and weight of the structural members, and can be executed with reduced construction time and labor compared to internal retrofitting approaches such as additional steel reinforcement or internal FRP bars. Furthermore, the external placement of the ropes allows for continuous confinement action along the joint region without disrupting the internal steel cage, enabling improved force transfer paths and more uniform stress distribution. A qualitative cost estimate of the proposed strengthening method is provided to give the reader an overview of its economic viability compared to common upgrading techniques such as externally bonded FRP laminates or steel jacketing. Based on indicative market prices, the cost of the C-FRP rope and sheet configuration used in the present study is estimated at approximately EUR 85–110 per meter of joint length, including materials and labor, depending on the project scale and site conditions. This cost is generally lower than that of steel jacketing due to the material's weight, welding requirements, and the need for corrosion protection—and comparable to or slightly higher than conventional FRP sheet strengthening, while offering superior stiffness retention and energy dissipation capacity. These practical benefits, combined with the experimentally confirmed improvements in strength, ductility, and energy dissipation, underline the suitability of the method for upgrading deficient RC joints in service without significant disruption to building use [25,26,34–36]. The intervention is minimally invasive, does not alter the geometry or weight of the structural elements, and can be applied to existing RC frames without major service disruption. The experimental results confirm that the combined use of X-shaped C-FRP ropes and externally bonded C-FRP sheets offers a robust, efficient, and practical solution for retrofitting RC beam–column joints. Beyond the demonstrated gains in strength, ductility, stiffness retention, and energy dissipation, the method stands out for its minimal invasiveness, adaptability to different joint configurations, and economic viability. These advantages highlight its strong potential for large-scale application in seismic retrofitting programs, providing a reliable pathway to extend the service life of existing RC structures and to enhance their resilience against future earthquakes.

Author Contributions: Conceptualization, C.K. and E.G.; methodology, E.G.; validation, C.K. and E.G.; investigation, E.G.; data curation, E.G.; writing—review and editing, C.K. and E.G.; visualization, E.G.; project administration, C.K. All authors have read and agreed to the published version of the manuscript.

Funding: This research received no external funding.

Data Availability Statement: Data available on request.

Acknowledgments: We would like to thank the company SIKA HELLAS SA (Athens, Greece) for the supply and free disposal of the needed FRP materials.

Conflicts of Interest: The authors declare no conflicts of interest.

References

1. Bakis, C.E.; Bank, L.C.; Brown, V.L.; Cosenza, E.; Davalos, J.F.; Lesko, J.J.; Machida, A.; Rizkalla, S.H.; Triantafillou, T.C. Fiber-reinforced polymer composites for construction—State-of-the-art review. *J. Compos. Constr.* **2002**, *6*, 73–87. [CrossRef]
2. Antonopoulos, C.P.; Triantafillou, T.C. Experimental investigation of FRP-strengthened RC beam-column joints. *J. Compos. Constr.* **2003**, *7*, 39–49. [CrossRef]
3. Al-Salloum, Y.A.; Elsanadedy, H.M.; Alsayed, S.H.; Iqbal, R.A. Seismic performance of RC beam–column joints upgraded with FRP sheets. *J. Compos. Constr.* **2012**, *16*, 74–90. [CrossRef]
4. *ACI 440.2R-08*; Guide for the Design and Construction of Externally Bonded FRP Systems for Strengthening Concrete Structures. ACI Com-mittee 440. American Concrete Institute: Farmington Hills, MI, USA, 2008.

5. Ehsani, M.R.; Saadatmanesh, H.; Tao, S. Design recommendations for flexural strengthening of RC beams with FRP plates. *ACI Struct. J.* **1993**, *90*, 34–41.
6. Bousias, S.N.; Spadea, G.; Triantafillou, T.C. Seismic retrofitting of beam–column joints using carbon-FRP jacketing. *ACI Struct. J.* **2007**, *104*, 287–296.
7. Cosenza, E.; Manfredi, G.; Realfonzo, R. Behavior and modeling of bond of FRP rebars to concrete. *J. Compos. Constr.* **1997**, *1*, 40–51. [CrossRef]
8. Bencardino, F.; Condello, A.; Spadea, G.; Swamy, R.N. Experimental performance of RC beams strengthened with FRP materials. *Compos. Struct.* **2010**, *92*, 2066–2077. [CrossRef]
9. El-Amoury, T.; Ghobarah, A. Seismic rehabilitation of beam–column knee joints using GFRP sheets. *Eng. Struct.* **2002**, *24*, 1397–1407. [CrossRef]
10. Tsonos, A.G. Effectiveness of CFRP jackets and RC jacketing in post-earthquake and pre-earthquake retrofitting of RC beam–column subassemblages. *Eng. Struct.* **2007**, *29*, 1216–1232.
11. *ACI 318-19*; Building Code Requirements for Structural Concrete. ACI Committee 318. American Concrete Institute: Farmington Hills, MI, USA, 2019.
12. Pantelides, C.P.; Volnyy, V.A.; Reaveley, L.D. Performance-Based Design of Precast Concrete Bridge Columns Using Fiber-Reinforced Plastic Jackets. *ACI Struct. J.* **2008**, *105*, 478–486.
13. Bousias, S.N.; Verzeletti, G.; Fardis, M.N.; Pavese, A. Lateral stiffness of RC structures under cyclic displacements. *J. Struct. Eng.* **1995**, *121*, 583–594.
14. Tsonos, A.G. Effectiveness of CFRP jackets and concrete jackets in retrofitting of beam–column subassemblages. *J. Earthq. Eng.* **2008**, *12*, 653–675.
15. Tsonos, A.G. Cyclic load behavior of reinforced concrete beam–column subassemblages upgraded with carbon fiber reinforced polymers. *J. Struct. Eng.* **2007**, *133*, 1309–1318.
16. Bousias, S.N.; Biskinis, D.E.; Fardis, M.N. Deformation capacity of members and joints of RC frames. *J. Struct. Eng.* **2004**, *130*, 1911–1924.
17. Golias, M.; Karayannis, C.G. Full-scale Experimental Testing of RC Beam-column Joints Strengthened using CFRP Ropes as External Reinforcement. *Eng. Struct.* **2022**, *250*, 113305. [CrossRef]
18. Golias, E.; Zapris, A.G.; Kytinou, V.K.; Kalogeropoulos, G.I.; Chalioris, C.E.; Karayannis, C.G. Effectiveness of the novel Rehabilitation Method of Seismically Damaged RC Joints using C-FRP ropes and Comparison with widely applied Method using C-FRP sheets—Experimental Investigation. *Sustainability* **2021**, *13*, 6454. [CrossRef]
19. Parvin, A.; Granata, P. Investigation of externally bonded FRP composites for retrofit of concrete structures. *J. Compos. Constr.* **2000**, *4*, 145–152.
20. Prota, A.; Nanni, A.; Manfredi, G. Experimental investigation of FRP-strengthened RC joints. *J. Compos. Constr.* **2003**, *7*, 95–103.
21. Mukherjee, A.; Joshi, M. FRPC reinforced concrete beams under direct shear. *Constr. Build. Mater.* **2005**, *19*, 295–301. [CrossRef]
22. Khalifa, A.; Nanni, A. Rehabilitation of rectangular simply supported RC beams with shear deficiencies using CFRP composites. *Constr. Build. Mater.* **2000**, *14*, 153–162. [CrossRef]
23. Pantelides, C.P.; Reaveley, L.D.; Volnyy, V.A. Seismic retrofit of reinforced concrete bridge columns with FRP composites. *J. Compos. Constr.* **2002**, *6*, 10–16.
24. Antonopoulos, C.P.; Triantafillou, T.C. Analysis of FRP-strengthened RC beam–column joints. *J. Compos. Constr.* **2002**, *6*, 41–51. [CrossRef]
25. Karayannis, C.G.; Sirkelis, G.M. Strengthening and rehabilitation of RC beam–column joints using carbon-FRP jacketing and epoxy resin injection. *Earthq. Eng. Struct. Dyn.* **2008**, *37*, 769–790. [CrossRef]
26. Karayannis, C.; Golias, E.; Kalogeropoulos, G.I. Influence of Carbon Fiber-Reinforced Ropes Applied as External Diagonal Reinforcement on the Shear Deformation of RC Joints. *Fibers* **2022**, *10*, 28. [CrossRef]
27. Prota, A.; Nanni, A.; Manfredi, G.; Cosenza, E. Selective upgrade of beam–column joints with composites. *ACI Struct. J.* **2004**, *101*, 699–707.
28. Golias, E.; Cotsovos, D. Assessing the performance of existing RC beam-column Joints C-FRP. In Proceedings of the 9th ECCOMAS Thematic Conference on Computational Methods in Structural Dynamics and Earthquake Engineering (COMPDYN 2023), Athens, Greece, 12–14 June 2023. [CrossRef]
29. Golias, E.; Touratzidis, P.; Karayannis, C.G. Seismic Response of RC Beam-Column Joints Strengthened with FRP ROPES, Using 3D Finite Element: Verification with real Scale Tests. *CivilEng* **2024**, *5*, 395–419. [CrossRef]
30. Xu, B.; Wang, R.; Zhou, K.; Zhou, X.; Xu, T.; Bian, Q. Research on the physical characteristics of a novel modified foamed cement slurry with non-foamed PVA material. *Constr. Build. Mater.* **2025**, *459*, 139710. [CrossRef]
31. Santarsiero, G.; Masi, A. Seismic upgrading of wide beam-column joints using steel jacketing. *Buildings* **2020**, *10*, 203. [CrossRef]
32. Kinjawadekar, T.A.; Patil, S.; Nayak, G. A Critical Review on Glass Fiber-Reinforced Polymer Bars as Reinforcement in Flexural Members. *J. Inst. Eng. India Ser. A* **2023**, *104*, 501–516. [CrossRef]

33. Szymczak-Graczyk, A.; Ksit, B.; Laks, I. Operational Problems in Structural Nodes of Reinforced Concrete Constructions. *IOP Conf. Ser. Mater. Sci. Eng.* **2019**, *603*, 032096. [CrossRef]
34. De Lima, L.R.O.; da Silva, L.S.; Vellasco, P.C.G.da S.; de Andrade, S.A.L. Experimental evaluation of extended endplate beam-to-column joints subjected to bending and axial force. *Eng. Struct.* **2004**, *26*, 1333–1347. [CrossRef]
35. Pantelides, C.P.; Gergely, J. Seismic Retrofit of RC Bridge Pier with CFRP Composite Jackets. *J. Compos. Constr.* **2002**, *6*, 1–14.
36. Al-Salloum, Y.A.; Almusallam, T.H. Seismic response of interior RC beam–column joints strengthened with FRP sheets. *J. Compos. Constr.* **2011**, *15*, 213–226.

Disclaimer/Publisher's Note: The statements, opinions and data contained in all publications are solely those of the individual author(s) and contributor(s) and not of MDPI and/or the editor(s). MDPI and/or the editor(s) disclaim responsibility for any injury to people or property resulting from any ideas, methods, instructions or products referred to in the content.